Lab on a Chip



Cite this: DOI: 10.1039/c1lc20701f

www.rsc.org/loc

PAPER

# Isolation of prostate tumor initiating cells (TICs) through their dielectrophoretic signature

**Alireza Salmanzadeh,[ab] Lina Romero,[c] Hadi Shafiee,[d] Roberto C. Gallo-Villanueva,[a] Mark A. Stremler,[b] Scott D. Cramer[c] and Rafael V. Davalos*[ab]**

***Received 29th July 2011, Accepted 20th October 2011***
**DOI: 10.1039/c1lc20701f**

In this study, the dielectrophoretic response of prostate tumor initiating cells (TICs) was investigated in a microfluidic system utilizing contactless dielectrophoresis (cDEP). The dielectrophoretic response of prostate TICs was observed to be distinctively different than that for non-TICs, enabling them to be sorted using cDEP. Culturing the sorted TICs generated spheroids, indicating that they were indeed initiating cells. This study presents the first marker-free TIC separation from non-TICs utilizing their electrical fingerprints through dielectrophoresis.



## Introduction

Tumor initiating cells (TICs) are cells from within an existing tumor that possess the ability to generate a new tumor that exhibits a similar histopathology as the tumor from which it was derived.[1] Isolating these tumor initiating cells is the first step towards understanding their role in the pathogenesis and progression of cancer and is critical for the development of improved cancer-specific therapies. However, current efforts in this direction are hampered by the lack of a suitable method for isolating these cells that combines high throughput with rapid results. Most methods currently rely on time-consuming labeling of surface marker expression followed by cell sorting *via* flow cytometry.[2,3]

Dielectrophoresis (DEP), the motion of a particle due to its polarization in the presence of a non-uniform electric field, can be used to differentiate between cells based on their intrinsic properties.[4] The dielectrophoretic force is a function of cell volume and polarization, the conductivity and permittivity of the surrounding media, and the frequency and spatial gradients of the magnitude of the applied electric field.[4] When subjected to the same electric field, cells with different dielectric properties may experience different dielectrophoretic forces. Several DEP applications have effectively demonstrated selective concentration of specific cell populations based on their size, shape, internal structure, and electrical properties. A few pertinent examples include the separation of human leukemia cells from red blood cells,[5] human breast cancer cells from blood,[6] human monocytic cells from peripheral blood mononuclear cells (PMBC),[7] red blood cells from debris,[8] poly-dispersed liposome suspensions,[8] cancer cells from CD34+ hematopoietic stem cells,[9] DNA and protein,[10] neuroblastoma cells from HTB glioma cells,[7] a putative stem cell population from an enzyme-digested adipose tissue,[11] cervical carcinoma cells,[12] live yeast cells from dead,[13,14] and malaria-infected cells from blood.[15] This study is the first use for DEP for the separation of tumor initiating cells from non-initiating cells.

Traditionally, DEP is applied with the use of an interdigitated electrode array patterned on the surface of a silicon wafer slide under a microfluidic channel through which the sample fluid passes. The electrode array produces the nonuniform electric field needed to drive the dielectrophoretic force. Although this has been a very successful technique for the manipulation, separation, and enrichment of bioparticles,[16,17] it has some difficulties such as bubble formation (due to electrolysis), electrode fouling and delamination, and expensive fabrication.[18,19] Modified DEP techniques, such as insulator-based dielectrophoresis (iDEP) have been developed to overcome many of the drawbacks of conventional DEP techniques. In iDEP, insulating obstacles are straddled between two electrodes to create a non-uniform electric field.[20] iDEP also employs microdevices fabricated using simple etching techniques, allowing mass production.[21–24] Although electrode fouling and delamination are eliminated, sending an electric current across the sample fluid in iDEP still results in electrolysis and also induces a large temperature increase in highly conductive biological samples that could damage the cells. A recent review of iDEP can be found in ref. 25.

The contactless dielectrophoresis (cDEP) technique capitalizes on the sensitivity of dielectrophoresis while eliminating many of its challenges. In cDEP, an electric field is created in the sample channel using electrodes inserted into two other microchannels (filled with conductive solution) that are separated from the sample channel by thin insulating barriers (Fig. 1(a)–(b)). These

[a]*Bioelectromechanical Systems Laboratory, School of Biomedical Engineering and Sciences, Virginia Tech–Wake Forest University, Blacksburg, VA, 24061, USA. E-mail: davalos@vt.edu; Tel: +1-540-998-9197*
[b]*Engineering Science and Mechanics Department, Virginia Tech, Blacksburg, VA, 24061, USA*
[c]*Department of Pharmacology, University of Colorado Denver, Aurora, CO, 80045, USA*
[d]*Center for Biomedical Engineering, Department of Medicine, Brigham and Women's Hospital, Harvard Medical School, Boston, MA, 02115, USA*

insulating barriers exhibit a capacitive behavior, and therefore an electric field can be produced in the sample channel by applying an AC field across the barriers. The geometry of the insulating barriers and insulating structures, *e.g.*, an array of insulating posts, within the sample channel can be customized to create devices which exhibit high sensitivity towards specific cell types. The side channels and the fluidic channels are fabricated on the same layer, and there is no need for electrode patterning; thus, fabrication of the cDEP microdevices has a relatively low cost and is readily amenable to mass fabrication techniques such as hot embossing and injection molding. The ability of cDEP to isolate THP-1 human leukemia monocytes from a heterogeneous mixture of live and dead cells,[26] to isolate cancer cells from erythrocytes,[27] and to separate breast cancer cells based on their metastatic stage[28] has been demonstrated recently.

The absence of a contact between the electrodes and the sample inside the fluidic channels avoids any contaminating effects the electrodes may have on the sample,[29] making cDEP an ideal "isolate-and-culture" platform for investigating the biological processes of a target cell type in animal models. Moreover, in contrast to techniques such as flow cytometry (*e.g.* fluorescence activated cell sorting (FACS)[30]), chemically functionalized pillar-based microchips,[31] or magnetic bead cell separation (*e.g.* magnetic-activated cell sorting (MACS)[32]), antibodies are not used in this cDEP cell identification technique.

Previous works with human prostate cancer cell lines and with primary human prostate samples have identified several markers for TICs. These markers include increased expression of cell surface proteins such as CD133, CD44, and $\alpha 2\beta 1$ integrin. Data from other tissue types also support the use of aldehyde dehydrogenase (ALDH), which can be measured by a fluorescent substrate, as a marker for TICs. It has been shown that the number of ALDH+ cells increases in tumor derived samples, consistent with its expression being associated with TICs.[33,34]

In this study, we have investigated the dielectric response of prostate tumor initiating cells (TICs) utilizing contactless dielectrophoresis (cDEP). A 1 mm wide cDEP device was used to characterize the dielectrophoretic response of prostate TICs. Two higher throughput devices, each 5 mm wide, were used in parallel to separate TICs from non-TICs and analyze the sample off-chip. Our results show that TICs have distinctively different dielectrophoretic properties than non-TICs and demonstrate that the voltage required to completely trap the cells in the collection array is different for the two cell types. Our results with the two wider devices verified cell viability and enabled us to culture the sorted cells. Unsorted samples of prostate cancer cells were separated

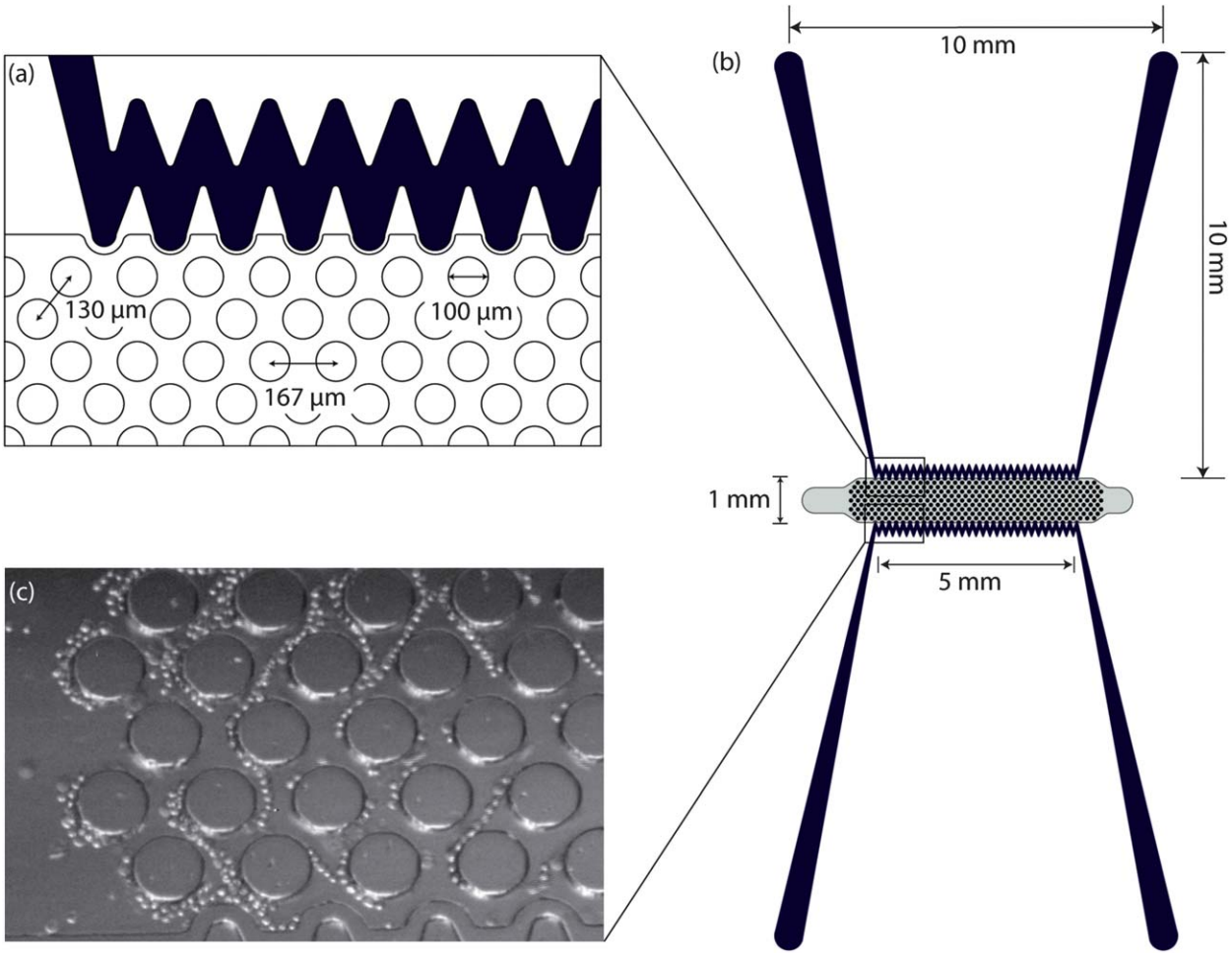


**Fig. 1** Top view schematic and dimensions of (a) a section of microchannels and pillars and (b) cDEP microdevice. (c) Trapped cells at 600 kHz and 129 $V_{rms}$.

 

using our cDEP device based on their dielectrophoretic response and subsequently cultured. Only the cells with a DEP response indicating they were TICs generated spheroids once cultured, which is indicative of tumor initiating cells.

### Theory

The time-average DEP force acting on a spherical particle in a non-uniform electric field is given by[4]

$$\vec{F}_{DEP} = 2\pi\varepsilon_m r^3 Re\left\{\frac{\varepsilon_p^* - \varepsilon_m^*}{\varepsilon_p^* + 2\varepsilon_m^*}\right\}\nabla(\vec{E}_{rms}\cdot\vec{E}_{rms}), \quad (1)$$

where $\varepsilon$ and $\varepsilon^*$ are the real and complex permittivity of the particle $p$ or suspending medium $m$, $r$ is the radius of the particle, and $\vec{E}_{rms}$ is the root mean square of the electric field. The complex permittivity is defined as

$$\varepsilon^* = \varepsilon - \frac{j\sigma}{\omega}, \quad (2)$$

where $\varepsilon$ and $\sigma$ are the real permittivity and conductivity, $j^2 = -1$, and $\omega$ is the radial frequency of the electric field. $(\varepsilon_p^* - \varepsilon_m^*)/(\varepsilon_p^* + 2\varepsilon_m^*)$ has been defined as Clausius-Mossotti factor,[4]

$$K(\varepsilon_p^*, \varepsilon_m^*) = \frac{\varepsilon_p^* - \varepsilon_m^*}{\varepsilon_p^* + 2\varepsilon_m^*}. \quad (3)$$

The magnitude of $K$ can vary from $-0.5$ to 1. Depending on he sign of $K$, the dielectrophoretic force can be either positive, in which case it is directed towards the high electric field gradient region, or negative, in which case it is directed towards the low electric field gradient region. This dependence is related to the polarizability of the particle with respect to the surrounding medium. The frequency at which the dielectrophoretic force is zero is called the crossover frequency *i.e.*, the frequency at which the real part of $K$ changes sign, $Re\ \{K(\varepsilon^*_p,\varepsilon^*_m)\} = 0$.

As particles move under the influence of the dielectrophoretic force, they interact with the surrounding fluid and experience a hydrodynamic force. Assuming a relatively high medium viscosity, $\eta$, and that the particles are small, spherical, and are moving with a relatively low velocity, the hydrodynamic force can be approximated as Stokes' drag, which is given by

$$\vec{F}_{Drag} = 6\eta r\pi(\vec{u}_p - \vec{u}_f), \quad (4)$$

where $r$ is the particle radius, $\vec{u}_p$ is the velocity of the particle, and $\vec{u}_f$ is the medium velocity. Then the translational velocity of the particle can be estimated by a balance between the dielectrophoretic force and Stokes' drag force on a particle,

$$\vec{u}_p = \frac{\vec{F}_{DEP}}{6\eta r\pi} + \vec{u}_f \quad (5)$$

This standard approach to modeling particle motion in DEP ignores the inertia of the particle.[35]

## Material and methods

### Device layout

Fig. 1 shows the top view schematic of the 1 mm wide microdevice. Electrode channels, which are approximately 1 cm long, are separated from the fluidic channel by 20 μm PDMS barriers. Insulating pillars of 100 μm in diameter have been used in the fluidic channel to create the nonuniformity of the electric field and enhance the dielectrophoretic force.

This 1 mm wide device was used to compare the electrical properties of ALDH+ cells (TICs) and ALDH− cells (non-TICs). However, since the 1 mm wide device has a very low throughput (0.02 mL $h^{-1}$) it is not practical for taking cells off the chip in the quantities necessary for evaluation of cell viability and for culturing cells after the DEP experiments. On the other hand, due to microscopy limitations, the onset and complete trapping of cells can be accurately observed only in the 1 mm wide design since the narrower device allows simultaneous visualization of the entire width. The two devices that were 5 mm wide operate in parallel (0.2 mL $h^{-1}$ in total) which allows collection of cells. The flow rate used in the wider devices produced the same average flow velocity as in the 1 mm device (110 μm $s^{-1}$). Moreover, the applied voltage has been adjusted using computational modeling for the 5 mm device to produce the same DEP force as the 1 mm device at a specific frequency. Thus, the cells will exhibit the same behavior in both devices, while increasing the throughput of the system by using the two parallel 5 mm wide devices.

### Microdevice fabrication

A silicon master stamp was fabricated on a <100> silicon substrate using Deep Reactive Ion Etching (DRIE) process. The scalloping effect, side wall roughness due to the DRIE etching method, which is detrimental to the stamping process, was removed by a 5 min wet etching using tetramethylammonium hydroxide (TMAH) 25% at 70 °C. A thin layer of Teflon was then deposited on the silicon master using DRIE system, which makes the stamping process easier. The liquid phase PDMS, made by mixing the PDMS monomers and the curing agent in a 10 : 1 ratio (Sylgrad 184, Dow Corning, USA), was then poured onto the silicon master and cured for 45 min at 100 °C. The cured PDMS was removed and fluidic connections were punched through the PDMS with blunt needles (Howard Electronic Instruments, USA). The PDMS replica was bonded with clean glass slides after treating with air plasma for 2 min.

### Experimental set-up

The two side channels were filled with Phosphate Buffered Saline (PBS) having an electrical conductivity of 1.4 S $m^{-1}$, and aluminum electrodes were placed in the reservoirs connected to the side channels. A 1 mL syringe fastened to a microsyringe pump (Harvard Apparatus Syringe Pumps, Plymouth Meeting, PA, USA) was connected to the inlet of the device through thin-walled Teflon tubing (Cole-Parmer Instrument Co., Vernon Hills, IL). To prevent bubble formation in the microchannels, the microdevices were put in vacuum for 30 min before running the experiments.

Once the main channel was primed with the cell suspension, the syringe pump was set to 0.02 mL $h^{-1}$ for the 1 mm wide device or 0.2 mL $h^{-1}$ for the two parallel 5 mm wide devices. This flow rate was maintained for 5 min prior to the experiments to have a steady flow. An inverted epifluorescence video microscope for microfluidics model SVM340 (LabSmith, Livermore, CA, USA),

equipped with a color camera, was used to monitor the cells flowing through the main channel, and the dielectrophoretic behavior of the cells were recorded as pictures and videos by using the software uScope (LabSmith, Livermore, CA, USA). A 4× objective was used for all experiments. The microscope requires the use of a personal computer for its operation.

Percentage of trapping of the cells was calculated by recording the outlet before and after turning on the electric field, and the number of cells leaving the post arrangement was counted manually in each case. To determine whether or not some cells are trapped due to fouling, several control experiments were run without applying an electric field and the number of cells entering the channel were counted and compared to the number of cells leaving the channel per unit of time. Although new devices were used for each set of the experiments, it was found that cell fouling was negligible and trapping was a result only of the dielectrophoretic force acting on the cells.

### Electrical equipment

AC electric fields were applied to the microfluidic devices using a combination of waveform generation and amplification equipment. Waveform generation was performed by a function generator (GFG-3015, GW Instek, Taipei, Taiwan) where the output was then fed to a wideband power amplifier (AL-50HF-A, Amp-Line Corp., Oakland Gardens, NY). A high-voltage transformer was then used to step-up the voltage of the signal before it was applied to the microfluidic device. The capacitive nature of the dielectric barriers that separate the electrodes from the sample fluid in the main microfluidic channel indicates that the magnitude of the electric field in the main channel was frequency dependent.[27]

### Cell culturing and cell preparation for flow cytometry

Human prostate cancer cells, PC3, were grown on 10 cm dishes, using Roswell Park Memorial Institute (RPMI) medium (Invitrogen cat. 11875-093), 10% fetal bovine serum (FBS) (Gemini Bio-products cat. 900-108), and 1% Penicillin/Streptomycin (P/S). In order to prepare the cells for flow cytometry, cells were trypsinized, spun to collect, and the pellet was resuspended in Aldefluor assay buffer (filter sterilized). After counting the cells, the cell dilution was prepared to achieve $1 \times 10^6$ cells $mL^{-1}$ and transferred to an eppendorf tube. Then, cells were incubated with Aldefluor substrate for 45 min at 37 °C, with or without Diethylaminobenzaldehyde (DEAB) inhibitor. Following incubation all samples were centrifuged for 5 min at 250 × g and the supernatant was removed. The cell pellet was resuspended in 500 μL Aldefluor assay buffer and placed at 4 °C before flow cytometry process.[33]

### Flow cytometry

Flow cytometry was used to isolate cells with putative markers of TICs to use them for the characterization of the cells dielectric properties. Single-cell suspensions of the PC3 cells were labeled with BODIPY®-aminoacetaldehyde (Aldefluor, for ALDH) as was explained in the cell preparation for the flow cytometry section. DEAB (ALDH inhibitor) was used for ALDH control in separate incubations to validate specificity. The labeled cells and their controls were sorted in an Aria cell sorter in the flow cytometry core facility of the Wake Forest University Comprehensive Cancer Center. Fig. 2 shows representative data from PC3 cells for ALDH expression. Data indicates that approximately 15.4% of cells specifically express ALDH.

### Protaspheres culturing

Sorted cells by cDEP were cultured with concentration of $1 \times 10^3$ cells $mL^{-1}$ in 10-cm low-attach dish (Fisher Scientific Co. 05-539-101) by adding 10 mL of Endothelial Cell Basal Medium (EBM) media with the following supplements: 100 mL of EBM (Lonza CC-3121) supplemented with 2 mL of B27 (Gibco 17504044) with a concentration of 50X (final concentration of 2%), 100 μL of Insulin (5mg $mL^{-1}$, Invitrogen, Core Lab) with a concentration of 4 mg $mL^{-1}$ (final concentration of 4 μg $mL^{-1}$), 20 μL of EGF (Fisher CB 40001) with a concentration of 100 μg $mL^{-1}$ (final concentration of 20 ng $mL^{-1}$), and 100 μL of FGF (Invitrogen PH60024) with a concentration of 20 μg $mL^{-1}$ (final concentration of 20 ng $mL^{-1}$). Spheroids were collected after 2 to 3 weeks and analyzed morphologically by quantifying the number and size of colonies formed.

### Cell viability

Cell viability was assessed using trypan blue and a hemacytometer. 0.1 ml of trypan blue stock solution was added to 1 ml of cells and the hemacytometer was loaded and examined immediately under a microscope at low magnification. Counting the number of blue stained cells and the number of total cells before and after experiments showed that cells' viability change was negligible after running experiments.

### Computational modeling

Computational modeling of spatial field gradients squared, $\nabla(\vec{E}_{rms} \cdot \vec{E}_{rms})$, and of the fluid motion were used to predict and optimize the device performance, specifically to reach a strong dielectrophoretic force, resulting in efficient trapping of cells.

The electric field distribution can be modeled computationally using a finite element method in Comsol Multiphysics 4.0 using the AC/DC module (Comsol Inc., Burlington, MA, USA). This

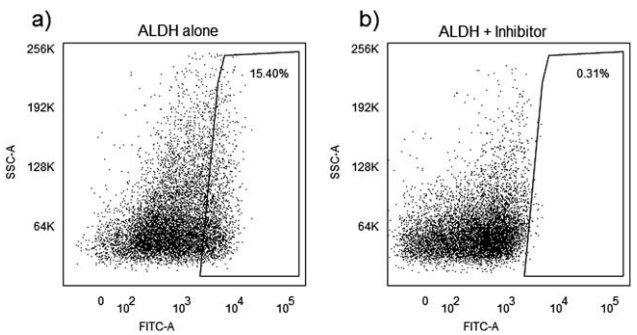


**Fig. 2** Identification of ALDH+ cells in a human prostate cancer cell line (PC3). 10,000 events were evaluated on a BD FACSAria cell sorter. Histograms show gated populations (a) without and (b) with Diethylaminobenzaldehyde (DEAB) inhibitor. Numbers in gated areas indicate the percent of the total population represented in the area.

is done by solving for the potential distribution, $\Phi$, using the governing equation $\nabla\cdot(\sigma^*\nabla\Phi) = 0$, where $\sigma^*$ is the complex conductivity ($\sigma^* = \sigma + j\omega\varepsilon$) of the sub-domains in the microfluidic devices. The boundary conditions used are prescribed uniform potentials at the inlet or outlet of the side channels. The computational models are used to predict where the strongest and weakest forces will occur and the range of voltages and frequencies these effects will be observed.

The electrical properties of PDMS used in the model have been reported by the manufacturer (Sylgard 184, Dow Corning, USA) as $\sigma_{PDMS} = 0.83 \times 10^{-12}$ S m$^{-1}$ and $\varepsilon_{PDMS} = 2.65$. The electrical conductivities of PBS and DEP buffer (8.5% sucrose [wt/vol], 0.3% glucose [wt/vol], and 0.725% [vol/vol] RPMI)[36] are $\sigma_{PDMS} =$ 1.4 S m$^{-1}$ and $\sigma_{DEP} = 0.01$ S m$^{-1}$, respectively, and their relative permittivities are $\varepsilon_{PBS} = \varepsilon_{DEP} = 80$. The electrical properties of PBS and DEP buffer are used for the side and main microfluidic channels, respectively. The distributed gradient of the electric field inside the main channel was investigated at frequencies of 100–600 kHz and voltages of 0–300 $V_{rms}$. Fig. 3(a) denotes $\nabla(\vec{E}_{rms}\cdot\vec{E}_{rms})$, at 300 $V_{rms}$ and 600 kHz in the 1 mm wide device. Insulating pillars located in the fluidic channel induce a large dielectrophoretic force by generating non-uniformities in the electric field.

The effect of the distance between the circular pillars on creating a strong and uniform gradient of the electric field intensity across the main channel was studied. It was observed that the gradient of the electric field has an inverse relation with the distance between the pillars (results not shown). However, this gap cannot be less than 30 μm as such devices will mechanically filter the prostate cancer cells due to their size. Thus, the device with a 30 μm gap between the pillars is optimum for our experiments.

$\nabla(\vec{E}_{rms}\cdot\vec{E}_{rms})$ was calculated for both, the 1-mm and the 5-mm wide devices. A comparison between $\nabla(\vec{E}_{rms}\cdot\vec{E}_{rms})$ on line A–B in Fig. 3(c) showed that $\nabla(\vec{E}_{rms}\cdot\vec{E}_{rms})$ generated by the 1 mm device is approximately 2.4 times higher than that of the 5 mm device. $\nabla(\vec{E}_{rms}\cdot\vec{E}_{rms})$ is proportional to the applied voltage squared, $V_{rms}^2$; thus, by applying $\sqrt{2.4}$ times higher voltage in the 5-mm device, achieves an equivalent $\nabla(\vec{E}_{rms}\cdot\vec{E}_{rms})$ as in the 1-mm device. Results for the magnitude of $\nabla(\vec{E}_{rms}\cdot\vec{E}_{rms})$ for the 1-mm device is shown on Fig. 3(a).

Fluid dynamics was also modeled to find the velocity field and shear rate in the main fluidic channel (Fig. 3(b)–(c)). No slip boundary conditions were applied to the walls of the channel and the pillars. The inlet velocity was set to 110 μm s$^{-1}$ based on the flow rate in the experiments and the outlet was set to no viscous stress (Dirichlet condition on the pressure). The Navier–Stokes equation was solved for an incompressible laminar flow. The viscosity and density of water, 0.001 Pa.s and 1000 kg m$^{-3}$, respectively, were used in the main fluidic channel (Fig. 3(b)–(c)). It can be seen in Fig. 3(c) that the computational result predicts the maximum shear rate in the device to be approximately two orders of magnitude less than the cell lysis limit ($\sim$ 5000 1/s[37,38]).

Fig. 3(d) presents the dimensionless values of $\nabla(\vec{E}_{rms}\cdot\vec{E}_{rms})$ and velocity on line A–B, which are proportional to the values of the dielectrophoretic and drag forces, respectively. The dimensionless velocity profiles show that by travelling between rows of pillars, the velocity increases and reaches its maximum value in the diagonal gap between the posts. $\nabla(\vec{E}_{rms}\cdot\vec{E}_{rms})$ has two maximum between each two row of pillars which are located

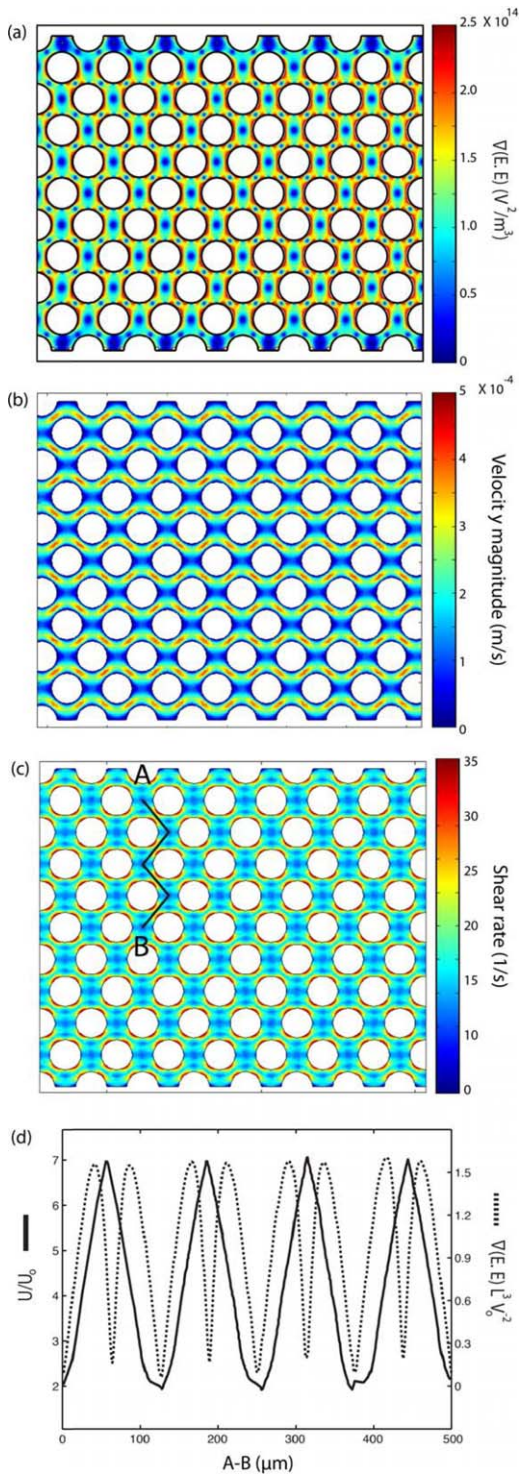


**Fig. 3** Computational modeling was used to predict the performance of the 1 mm-wide device. (a–c) Flow is from left to right and electrode channels are located on top and bottom of the simulated area. Surface plot of (a) the gradient of the electric field squared (V$^2$ m$^{-3}$) at 300 $V_{rms}$ and 600 kHz, (b) flow velocity magnitude (μm s$^{-1}$), and (c) shear rate (s$^{-1}$) in the fluidic channel. (d) Dimensionless values of velocity and $\nabla(\vec{E}_{rms}\cdot\vec{E}_{rms})$ on line A–B. Velocity, $U$, is nondimensionalized by inlet velocity, $U_o = 110$ μm s$^{-1}$ (left ordinate). $\nabla(\vec{E}_{rms}\cdot\vec{E}_{rms})$ (right ordinate) is nondimensionalized by applied voltage, $V_o$, and the distance between electrode channels (= 1 mm), which is equal to channel width.

approximately in the narrow gap between the insulators, and there is also a local minimum between these maximums. Minimum values of both velocity and $\nabla(\vec{E}_{rms} \cdot \vec{E}_{rms})$ on line A–B are located in the horizontal gap between two columns of pillars.

## Results and discussion

The DEP response of prostate cancer cells expressing ALDH+ (TICs) and ALDH- (non-TICs) was investigated separately to evaluate their dielectrophoretic response. Cells used were isolated and enriched by FACS and their signal parameters for DEP trapping was measured and recorded for the microfluidic platform described. It was observed that there was a great tendency for cells to move towards the high DEP regions in the main channel around the pillars and in the narrow region between them (Fig. 1(c)). Comparing with our numerical modeling, these results indicate that TICs were experiencing positive DEP force in the frequency range we applied in our microfluidic devices. The electrical properties of TICs are unknown and this is the first study that suggests that their electrical properties are different from non-TICs. Depending on the electrical conductivity and permittivity of the media, cell membrane, and other intrinsic properties of the cell, the polarized cell can be drawn away (negative DEP) or pulled towards (positive DEP) higher gradients of the field squared at different frequencies.

The voltages and frequencies of the applied signal for trapping of ALDH+ and ALDH- prostate cancer cells are reported in Fig. 4 (a)–(e). The frequency of the signal was set as indicated in each experiment, and the associated voltages required to observe i) trapping of the first cell (onset of trapping) and ii) trapping of all cells (complete trapping) were recorded. These results indicate that complete trapping of prostate TICs occurs at a lower voltage than that needed for complete trapping of non-TICs. Fig. 4(a)–(e) also shows that by increasing the frequency, the voltage required for trapping decreases. This decrease occurs because the magnitude of the electric field gradient increases by increasing the frequency due to the capacitive behavior of the barriers, so that the same DEP force can be achieved by applying a lower voltage.

One of the advantages of microelectrode-based DEP is its ability to operate across a wide frequency spectrum. This allows investigators to exploit the Clausius-Mossotti factor to its full extent and manipulate one cell population using positive DEP while simultaneously another with negative DEP. The capacitive nature of PDMS barrier limits applications of cDEP comparing to traditional DEP-techniques. In the cDEP devices presented here, typically, frequencies above 100 kHz are necessary to generate sufficient DEP forces to manipulate cells.[26] This generally limits the use of cDEP to methods which invoke a positive DEP response, since at lower frequencies, the voltage necessary to induce a DEP response is higher than the PDMS breakdown voltage (approximately 350 $V_{rms}$ for a 20 mm barrier[39]). However, Sano *et al.* have recently demonstrated a technique to improve the frequency response of cDEP devices, providing a nearly uniform DEP force over a spectrum between 3 kHz and 10 MHz.[27] Additionally, they have demonstrated that this technique can be used to manipulate mammalian cells using both positive and negative DEP.[40]

Ideally, the proposed device will selectively trap all ALDH+ cells while letting all ALDH- cells flow towards the outlet due to the difference in their dielectrophoretic properties. To evaluate the selectivity of the design, experiments with ALDH- cells were performed at voltages and frequencies for complete trapping of ALDH+ cells. Through these experiments, which were performed at the complete trapping voltages and frequencies of ALDH+ cells, 61.94% (sd = 6.79) of ALDH- cells at 600 kHz were trapped as is presented on Fig. 4(f).

It was observed, Fig. 4(a)–(e), that the difference between onset of trapping and complete trapping voltage required for ALDH+ cells is less than ALDH− cells. This difference also decreases with frequency when it is increased from 200 kHz to 600 kHz, specifically for ALDH+ cells, thus enhancing the separation of the cells. Therefore, separation of ALDH+ from ALDH− cells was performed only at a frequency of 600 kHz in the following experiments.

Generation of spheroids from cells derived from a number of tissues grown in a low-binding environment has been used to selectively propagate and enrich cells with enhanced stem cell properties. Furthermore, data suggests that spheroids from tumor cell populations are enriched with TIC properties. Therefore, a prostasphere assay was performed to evaluate sphere-forming abilities of the cDEP separated cells. Non-sorted PC3 cells were continuously injected into the cDEP microdevice at the flow rate of 0.2 mL $h^{-1}$ using a microsyringe pump and an electric field at 600 kHz and 300 $V_{rms}$ was generated to trap the cells by means of DEP. After 30 min, the voltage was decreased to 280 $V_{rms}$ ($\approx \sqrt{2.4} \times 179$ $V_{rms}$, where 179 $V_{rms}$ is the complete trapping voltage of ALDH+ cells at 600 kHz, see Fig. 4(e)) to release some cells while the rest were still immobilized in the areas of high DEP force around the pillars of the device. Cells that could have escaped the trapping area when the potential of 300 $V_{rms}$ was applied as well as those that were released when the voltage was decreased to 280 $V_{rms}$ were collected and cultured. Then, by decreasing the voltage to 150 $V_{rms}$ (complete trapping voltage for TICs) some other cells were released. It can be inferred from the results presented in Fig. 4 that most of the non-trapped and released cells are non-TICs, since the voltage for their complete trapping is higher than that for the TICs. Afterwards, the inlet fed was switched to cell-free DEP buffer for 15 min while the electric field was maintained at TIC trapping conditions to ensure all released cells exited the microdevice. Collection of the rest of the cells, which were expected to be enriched in TICs, was achieved by removing the electric field using DEP buffer as suspending medium.

The collected samples as well as non-sorted PC3 cells were cultured, used as the control experiment. Fig. 5 shows the formation of spheroids of the three groups of cells after 3 weeks. It can be seen that no large spheroid was observed in the dish containing cells which were released before or at 280 $V_{rms}$ (Fig. 5 (b)), evidence that the majority of these cells were non-TICs. The average size of these spheroids was 3143 $\mu m^2$ (sd = 1616) (n = 5). On the other hand, there were several large spheroids in the dish cultured with the cells that were released after turning off the electric field (Fig. 5(c)), which validates the presence of TICs. The average size of these spheroids was 54793 $\mu m^2$ (sd = 16424) (n = 6). The average size of unsorted PC3 cells (control) was 13951 $\mu m^2$ (sd = 7881) (n = 4). These results show that the average size of the cDEP enriched ALDH+ spheroids is 3.93 times larger than control, and 17.30 times larger than cDEP enriched ALDH- cells spheroids. Viability of the cells was also determined by trypan

 

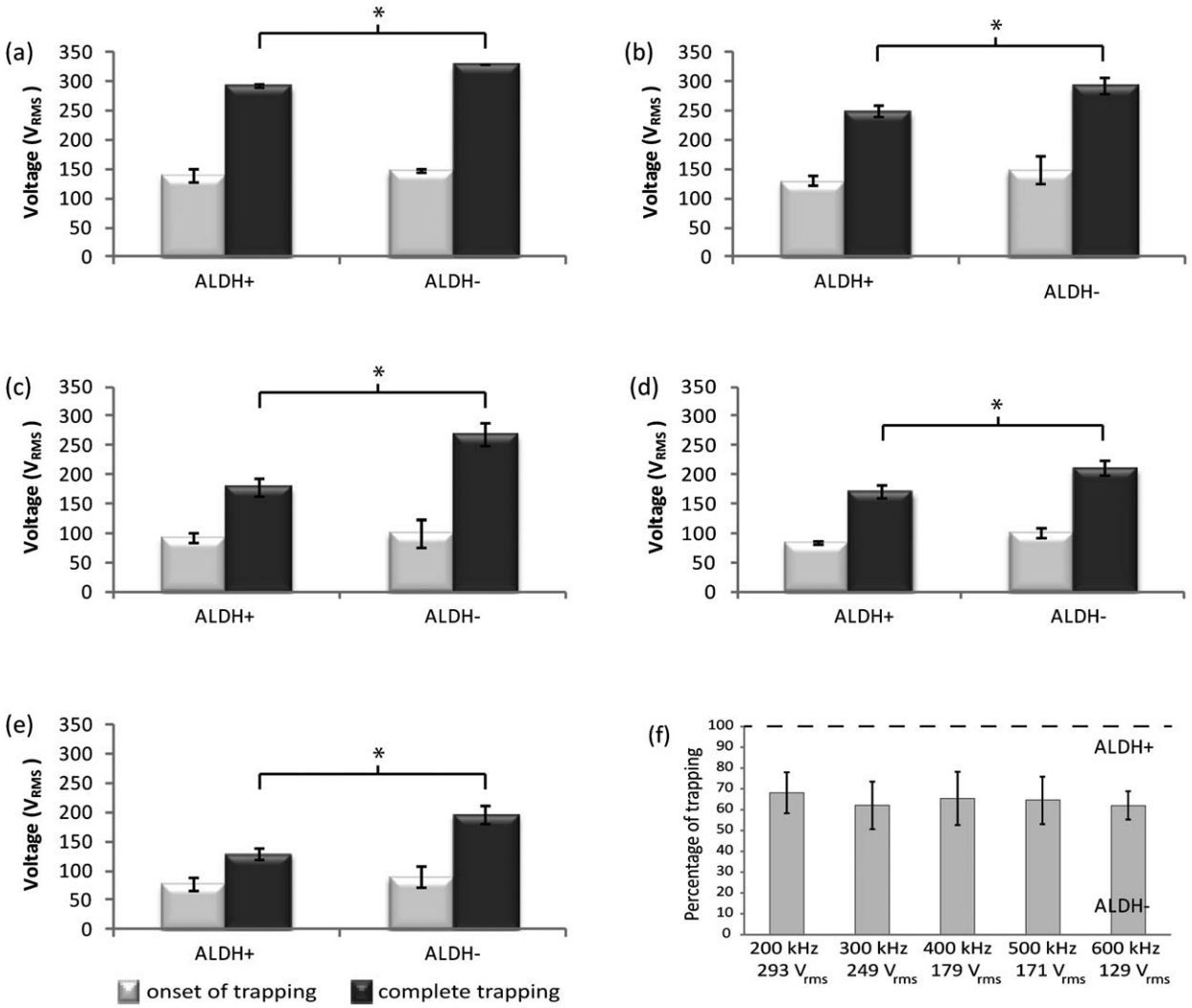


**Fig. 4** Voltage of trapping of ALDH+ and ALDH- cells at (a) 200 kHz, (b) 300 kHz, (c) 400 kHz, (d) 500 kHz, and (e) 600 kHz (n = 4). Light grey and dark grey bars present the onset of trapping and complete trapping, respectively. Complete trapping voltage of ALDH+ and ALDH− cells at each frequency are significantly different ($p < 0.005$), represented by *. (f) Percentage of trapping of ALDH- cells at 200–600 kHz at complete trapping voltage of ALDH+ cells.

blue exclusion before and after the experiments and no significant change in the cells viability was observed. These results are in agreement with the results presented in Fig. 4, demonstrating that TICs exhibit stronger DEP force than non-TICs at a specific frequency and voltage since their dielectrophoretic properties differ, and therefore lower voltages are needed to trap them. Our

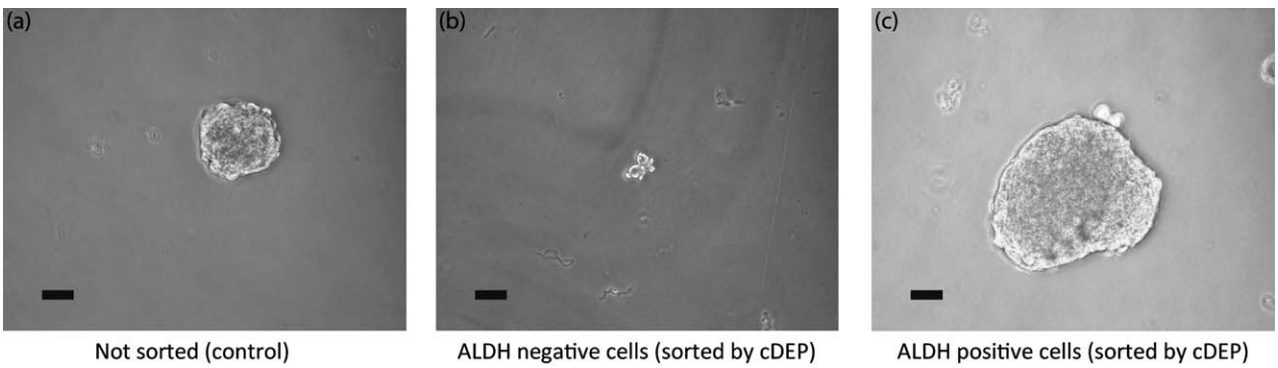


**Fig. 5** Photos of spheroids generated by culturing (a) unsorted PC3 cells (control), (b) released cells at 280 $V_{rms}$ (ALDH-), and (c) released cells after turning electric field off (ALDH+). Images are taken after 3 weeks at 20X magnification. Bars are 50 μm long.

data demonstrate that cells trapped with a cDEP signature associated with ALDH expression preferentially generate spheroids, consistent with our hypothesis. Future studies will further characterize these populations of cells for TIC marker expression and gene expression signatures.

It has been shown that membrane proteins can be associated to dielectric properties. For instance ABO-Rh antigens on the red blood cell membrane surface and traversing through it[41–43] and membrane alterations[44,45] can be identified. Moreover, the dielectric properties of the membrane can be extracted from the cells' DEP signatures. Thus, we hypothesize that one of the reasons that ALDH+ and ALDH− cells show different dielectric properties is that they have different proteins on their membrane surface. There is also a possibility that these proteins change the total electrical charge and the conductivity of the cell membrane in TICs versus non-TICs, although more in depth investigation is needed.

## Conclusions

The enrichment achieved by the presented device demonstrates the difference in the dielectrophoretic properties of prostate TICs and non-TICs. The difference between TICs and non-TICs might come from the differences of the membrane surface proteins of these cells and the electrical charge of these proteins. This difference can be used to isolate them by means of positive DEP, eliminating the necessity of extensive sample preparation (no antibody labeling) which is the other advantage of cDEP over other cell sorting techniques.

Another advantage of cDEP when compared to flow cytometry techniques, such as FACS, is that cDEP can be utilized to isolate probable subpopulations of cells by sorting populations at different voltages. Since current techniques cannot entirely isolate TICs from background, cDEP may offer an opportunity to identify the rare subpopulation(s) of ALDH+ cells that are the tumor initiating cells.

## Acknowledgements

This material is based upon work supported in part by the National Science Foundation under Grant No. EFRI 0938047 and by the Virginia Tech Institute for Critical Technology and Applied Science (ICTAS). The authors would like to thank the members of BEMS laboratory, especially Mike Sano for his help in experiments, Andrea Rojas for their help with editing this document, M. R. Makris, flow cytometry laboratory supervisor at College of Veterinary Medicine of Virginia Tech for helping in flow cytometry data analysis, and D. Maiti from Laboratory of Interdisciplinary Statistical Analysis at Virginia Tech for helping in data statistical analysis.

## References

1 T. Reya, S. Morrison, M. Clarke and I. Weissman, *Nature*, 2001, **414**, 105–111.
2 A. Collins, P. Berry, C. Hyde, M. Stower and N. Maitland, *Cancer Res.*, 2005, **65**, 10946–10951.
3 L. Patrawala, T. Calhoun-Davis, R. Schneider-Broussard and D. G. Tang, *Cancer Res.*, 2007, **67**, 6796–6805.
4 H. A. Pohl, *Dielectrophoresis: The behavior of neutral matter in nonuniform electric fields*, Cambridge University Press, Cambridge, 1978.
5 F. Becker, X. Wang, Y. Huang, R. Pethig, J. Vykoukal and P. Gascoyne, *J. Phys. D: Appl. Phys.*, 1994, **27**, 2659–2662.
6 H.-S. Moon, K. Kwon, S.-I. Kim, H. Han, J. Sohn, S. Lee and H.-I. Jung, *Lab Chip*, 2011, **11**, 1118–1125.
7 Y. Huang, S. Joo, M. Duhon, M. Heller, B. Wallace and X. Xu, *Anal. Chem.*, 2002, **74**, 3362–3371.
8 I.-F. Cheng, V. E. Froude, Y. Zhu, H.-C. Chang and H.-C. Chang, *Lab Chip*, 2009, **9**, 3193–3201.
9 M. Stephens, M. S. Talary, R. Pethig, A. K. Burnett and K. I. Mills, *Bone Marrow Transpl.*, 1996, **18**, 777–782.
10 S. Agastin, M. R. King and T. B. Jones, *Lab Chip*, 2009, **9**, 2319–2325.
11 J. Vykoukal, D. M. Vykoukal, S. Freyberg, E. U. Alta and P. R. C. Gascoyne, *Lab Chip*, 2008, **8**, 1386–1393.
12 J. Cheng, E. Sheldon, L. Wu, A. Uribe, L. Gerrue, J. Carrino, M. Heller and J. O'Connell, *Nat. Biotechnol.*, 1998, **16**, 541–546.
13 Z. Gagnon, J. Mazur and H.-C. Chang, *Lab Chip*, 2010, **10**, 718–726.
14 Y. Li, C. Dalton, H. J. Crabtree, G. Nilsson and K. V. I. S. Kaler, *Lab Chip*, 2007, **7**, 239–248.
15 P. Gascoyne, C. Mahidol, M. Ruchirawat, Jutamaad, Satayavivad, P. Watcharasit and F. F. Becker, *Lab Chip*, 2002, **2**, 70–75.
16 R. Pethig, *Biomicrofluidics*, 2010, **4**, 022811.
17 K. Khoshmanesh, S. Nahavandi, S. Baratchi, A. Mitchell and K. Kalantar-zadeh, *Biosens. Bioelectron.*, 2011, **26**, 1800–1814.
18 E. B. Cummings and A. K. Singh, *Anal. Chem.*, 2003, **75**, 4724–4731.
19 C. Chou, J. Tegenfeldt, O. Bakajin, S. Chan, E. Cox, N. Darnton, T. Duke and R. Austin, *Biophys. J.*, 2002, **83**, 2170–2179.
20 J. L. Baylon-Cardiel, N. M. Jesus-Perez, A. V. Chavez-Santoscoya and B. H. Lapizco-Encinas, *Lab Chip*, 2010, **10**, 3235–3242.
21 B. H. Lapizco-Encinas, S. Ozuna-Chacón and M. Rito-Palomares, *J. Chromatogr., A*, 2008, **1206**, 45–51.
22 B. A. Simmons, G. J. Mcgraw, R. V. Davalos, G. J. Fiechtner, Y. Fintschenko and E. B. Cummings, *MRS Bull.*, 2006, **31**, 120–124.
23 L. M. Barrett, A. J. Skulan, A. K. Singh, E. B. Cummings and G. J. Fiechtner, *Anal. Chem.*, 2005, **77**, 6798–6804.
24 P. Sabounchi, A. M. Morales, P. Ponce, L. P. Lee, B. a. Simmons and R. V. Davalos, *Biomed. Microdevices*, 2008, **10**, 661–670.
25 S. K. Srivastava, A. Gencoglu and A. R. Minerick, *Anal. Bioanal. Chem.*, 2011, **399**, 301–321.
26 H. Shafiee, M. B. Sano, E. A. Henslee, J. L. Caldwell and R. V. Davalos, *Lab Chip*, 2010, **10**, 438–445.
27 M. B. Sano, J. L. Caldwell and R. V. Davalos, *Biosens. Bioelectron.*, 2011, **30**, 13–20.
28 E. Henslee, M. B. Sano, A. Rojas, E. Schmelz and R. V. Davalos, *Electrophoresis*, 2011, **32**, 2523–2529.
29 A. Gencoglu and A. Minerick, *Lab Chip*, 2009, **9**, 1866–1873.
30 A. Lostumbo, D. Mehta, S. Setty and R. Nunez, *Exp. Mol. Pathol.*, 2006, **80**, 46–53.
31 S. Nagrath, L. V. Sequist, S. Maheswaran, D. W. Bell, D. Irimia, L. Ulkus, M. R. Smith, E. L. Kwak, S. Digumarthy, A. Muzikansky, P. Ryan, U. J. Balis, R. G. Tompkins, D. A. Haber and M. Toner, *Nature*, 2007, **450**, 1235–1239.
32 K. Kato and A. Radbruch, *Cytometry*, 1993, **14**, 384–392.
33 W. W. Barclay, L. S. Axanova, W. Chen, L. Romero, S. L. Maund, S. Soker, C. J. Lees and S. D. Cramer, *Stem Cells*, 2008, **26**, 600–610.
34 W. W. Barclay and S. D. Cramer, *Prostate*, 2005, **63**, 291–298.
35 H. Morgan and N. G. Green, *AC Electrokinetics: Colloids and Nanoparticles*, Research Studies Press, 2003.
36 L. A. Flanagan, J. Lu, L. Wang, S. A. Marchenko, N. L. Jeon, A. P. Lee and E. S. Monuki, *Stem Cells*, 2008, **26**, 656–665.
37 R. C. Skalak and S. Chien, *Handbook of Bioengineering*, McGraw-Hill, New York, 1987.
38 Y. C. Fung, N. Perrone and M. Anliker, *Biomechanics, Its Foundations and Objectives*, Prentice Hall, Englewood Cliffs, NJ, 1972
39 J. C. McDonald and G. M. Whitesides, *Acc. Chem. Res.*, 2002, **35**, 491–499.
40 M. B. Sano, E. A. Henslee, E. Schmelz and R. V. Davalos, *Electrophoresis*, 2011, **32**.
41 S. K. Srivastava, A. Artemiou and A. R. Minerick, *Electrophoresis*, 2011, **32**, 2530–2540.
42 S. K. Srivastava, P. R. Daggolu, S. C. Burgess and A. R. Minerick, *Electrophoresis*, 2008, **29**, 5033–5046.
43 K. M. L. a. A. R. Minerick, *Electrophoresis*, 2011, **32**, 2512–2522.
44 J. Oblak, D. Krizaj, S. Amon, A. Macek-Lebar and D. Miklavcic, *Bioelectrochemistry*, 2007, **71**, 164–171.
45 B. G. Hawkins, C. Huang, S. Arasanipalai and B. J. Kirby, *Anal. Chem.*, 2011, **83**, 3507–3515.

 